https://doi.org/10.5194/cp-2019-154
Preprint. Discussion started: 19 February 2020

Climate of the Past Discussions

A global climatology of the ocean surface during the Last Glacial Maximum mapped on a regular grid (GLOMAP)

André Paul[1], Stefan Mulitza[1], Rüdiger Stein[2], and Martin Werner[2]

[1] MARUM – Center for Marine Environmental Sciences and Department of Geosciences, University of Bremen, Bremen, Germany
[2]Alfred Wegener Institute, Helmholtz Centre for Polar and Marine Research (AWI), Bremerhaven, Germany

Correspondence: André Paul (apaul@marum.de)

Abstract. We present a climatology of the sea-surface temperature (SST) anomaly and the sea-ice extent during the Last Glacial Maximum (LGM, 23,000–19,000 years before present) mapped on a global regular 1°×1° grid. It is an extension of the Glacial Atlantic Ocean Mapping (GLAMAP) reconstruction of the Atlantic SST based on the results of the Multiproxy Approach for the Reconstruction of the Glacial Ocean Surface (MARGO) project and several recent estimates of the LGM sea-ice extent. Such a gridded climatology is highly useful for the visualization of the LGM climate, calculation of global and regional SST averages and estimation of the equilibrium climate sensitivity, as well as a boundary condition for atmospheric general circulation models. The gridding of the sparse SST reconstruction was done in an optimal way using the Data-Interpolating Variational Analysis (DIVA) software, which takes into account the uncertainty on the reconstruction and includes the calculation of an error field. The resulting Glacial Ocean Map (GLOMAP) confirmed the previous findings by the MARGO project regarding longitudinal and meridional SST differences that were greater than today in all oceans and an equilibrium climate sensitivity at the lower end of the currently accepted range.

1 Introduction

Gridded climatologies are useful for a number of purposes, for example, for visualizing present or past climate states, calculating global and regional averages, or evaluating climate models. Regarding the evaluation of climate models, unless data locations and model grid points coincide, we cannot quantify the data-model misfit without any sort of mapping. Thus, sparse data must be mapped onto the model grid by statistical methods (Schäfer-Neth et al., 2005; Marchal and Curry, 2008). Furthermore, a gridded sea-surface temperature (SST) climatology may serve as a boundary condition for atmospheric general circulation models (AGCMs) and enable a model evaluation that does not depend on the quality of a simulated SST climatology, allowing for another approach in comparing coupled climate models such as in the Paleo-Model Intercomparison Project (PMIP, e.g., Kageyama et al., 2017).

https://doi.org/10.5194/cp-2019-154
Preprint. Discussion started: 19 February 2020


Climate of the Past Discussions

A climate state of the past that is particularly useful for evaluating climate models is the Last Glacial Maximum (LGM, 19,000 to 23,000 years before present; Mix et al., 2001) cold period: The radiative perturbations due to changes in insolation, greenhouse gases and ice sheets are relatively well defined and the paleo-data coverage is comparitively dense and indicates a large response to the radiative forcing (Jansen et al., 2007; Masson-Delmotte et al., 2013). Previous work on a gridded SST climatology for the LGM includes the Climate: Long range Investigation, Mapping, and Prediction (CLIMAP) project (CLIMAP Project Members, 1981), the Glacial Atlantic Ocean Mapping (GLAMAP) SST reconstruction of the Atlantic SST (Sarnthein et al., 2003) and the Multiproxy Approach for the Reconstruction of the Glacial Ocean Surface (MARGO) (Kucera et al., 2005a). While CLIMAP and GLAMAP (Paul and Schäfer-Neth, 2003; Schäfer-Neth and Paul, 2004) provide seasonal reconstructions of the Earth's surface at the LGM mapped on a 2° grid, MARGO only performed a "pseudo gridding" by calculating 5° block averages (MARGO Project Members, 2009).

Here we present an ocean climatology of the sea surface during the LGM mapped on a global $1° \times 1°$ grid. This Glacial Ocean Map (GLOMAP) extends the gridded GLAMAP climatology to the global ocean based on the MARGO SST reconstruction. In addition, we included a more recent estimate of Southern Ocean summer sea-ice extent (Roche et al., 2012) and reconstructions of Arctic and North Pacific sea-ice extent using the IP25/PIP25 sea-ice proxy and phytoplankton-derived biomarkers (Xiao et al., 2015; Méheust et al., 2016; Méheust et al., 2018).

The sparse SST reconstruction, complemented with the reconstructed sea-ice boundaries in the northern and southern hemispheres, was gridded in an optimal way using the Data-Interpolating Variational Analysis (DIVA) method (Troupin et al., 2012). This method allows to take into account the uncertainty on the reconstruction and calculate an uncertainty field, which can be used as a weight in calculating uncertainty-weighted global and regional averages or for assessing the data-analysis mismatch. Originally developed for usually much denser oceanographic observations, the DIVA method proved to be capable of analyzing sparse paleo data as well.

2 Methods

2.1 Selecting LGM sea-ice extent reconstructions

For estimating LGM sea-ice extent, we made use of estimates of maximum and minimum sea ice extent in the Northern and Southern Hemispheres and added a physically reasonable seasonal cycle. As there are only few SST reconstructions in the high latitudes of either hemisphere, the information on past sea-ice coverage also served to fill in the gaps.

In line with earlier results obtained by the GLAMAP project (Sarnthein et al., 2003), the Nordic Seas were taken as ice-free during summer. Accordingly, we digitized sea-ice edges published by de Vernal et al. (2005, Fig. 10, upper left) and Kucera et al. (2005b, Fig. 25) for the Labrador Sea and Nordic Seas, Xiao et al. (2015, Fig. 7a) for the Barents Sea and Méheust et al. (2018, Fig. 9a) for the North Pacific Ocean. Similarly, we digitized sea-ice reconstructions by Gersonde et al. (2005, Fig. 4, maximum extent of winter sea ice "E-LGM-WSI" and sporadic occurrence of summer sea ice "E-LGM-SSI") and Roche et al. (2012, Fig. 4, bottom, Southern Ocean summer sea-ice extent "PROX.") for the Southern Hemisphere. If necessary, we re-projected them (e.g., from a polar stereographic or orthographic projection) to longitude and latitude. We

https://doi.org/10.5194/cp-2019-154
Preprint. Discussion started: 19 February 2020


Climate of the Past Discussions

connected them smoothly in each hemisphere and season and created sea-ice masks for summer and winter (note that the sea-ice reconstructions based on IP25/PIP25 by Xiao et al., 2015, and Méheust et al., 2018, apply to spring, but were in this study taken as an approximation to the winter sea-ice edge).

We created a seasonal cycle of sea-ice coverage as follows: At a given longitude, we assumed a sinusoidal cycle of the latitude of the sea ice edge (cf. Eisenman, 2010) between the maximum and minimum sea ice extent in either hemisphere.

2.2 Selecting LGM SST reconstructions

For consistency among the individual LGM estimates, we selected from the MARGO database (Kucera et al., 2005a; MARGO Project Members, 2009) only those that were based on the faunal transfer function technique. Dinocyst assemblages were only used south of the assumed winter sea-ice boundary at about 50°N (de Vernal et al., 2005; De Vernal et al., 2006). To this end, we extracted all dinoflagellate data assumed to be not affected by winter sea-ice cover in the Nordic Seas.

Each MARGO SST estimate is associate with an error that is equal to the product of the calibration error and a semi-quantitative "reliability index". The reliability index takes into account the number of samples, the quality of the age model and a possible lack of stationarity reflecting, for example, possible no-analogue situations and a known regional or sedimentological bias (MARGO Project Members, 2009). The calibration error ranges typically between 1 °C and 1.5 °C, and the reliability index ranges between 1 for high reliability and about 3.3 for low reliability. All errors were taken to reflect a $1\,\sigma$ confidence interval.

2.3 Gridding

We used version 4.7.1 (doi:10.5281/zenodo.836727) of DIVA (Troupin et al., 2012). The purpose of DIVA is to satisfy a variational principle that includes the magnitude of the data (anomalies) themselves as well as on the gradients, the variability and data-analysis misfits (Troupin et al., 2019, Eqs. 2.10 and 2.11). The general work flow of DIVA is summarized in Figure 1. The first step is to generate coast lines from a given topography. Based on the resulting coast lines, a finite-element mesh is created. Then first-guess values of the three analysis parameters (correlation length, signal-to-noise ratio and variance of background field) are estimated and an analytic covariance function is fit to the data, yielding a revised estimate of the correlation length. Finally, a generalized cross validation can be carried out to improve the signal-to-noise ratio and the variance of background field.

In our case, we used the glacial topography GLAC-1D at 21,000 years before present (cf. Tarasov et al., 2012; Briggs et al., 2014) to generate glacial coast lines and create a corresponding global finite-element mesh. The first-guess values of the correlation length and the signal-to-noise ratio were set to 10° and 1.0, respectively. The first-guess value of the variance of the background field was estimated from the foraminiferal SST reconstructions as 6.3 $(°C)^2$. We fitted the covariance function to the foraminiferal data for the nominal seasons January-February-March (JFM) and July-August-September (JAS) and obtained estimates of the correlation length of 9.2° and 10.2°, respectively. In the remainder of our study, we fixed the correlation length at a value of 10°. The generalized cross validation did not yield significantly different values for the signal-to-noise ratio and the variance of background field. To each data value, we assigned a relative weight, which was inversely proportional to the

https://doi.org/10.5194/cp-2019-154
Preprint. Discussion started: 19 February 2020


Climate of the Past Discussions

error (a large value corresponded to a high confidence) and normalized such that the sum over all inverse relative weights equaled the number of data points.

We performed two iterations in order to arrive at a final global gridded climatology of monthly SST:

1. In the first iteration, we concatenated all foraminiferal data and the dinoflagellate data for ice-free regions including their relative weights for JAS and JFM. We created seasonal (monthly) data from the JFM (taken as February) and JAS (taken as August) data using a sine function. We extracted the geographic positions marked as sea ice from the monthly masks of the reconstructed sea-ice extent and determined the local SST anomaly using a temperature of -1.8 °C for the LGM value and the World Ocean Atlas (WOA, 1998) at 10 m depth for the modern value. To each sea-ice covered data point we assigned an error of 2 °C that was chosen to be larger than the error of any individual LGM estimate from the MARGO database. Then we concatenated the seasonal (monthly) foraminiferal and dinoflagellate data and the local SST anomalies from the sea-ice reconstructions and normalized the individual errors such that the sum of all errors equaled one. Finally, we gridded the data for each month. We achieved continuity across the 0° meridian by adapting the method by Tyberghein et al. (2012) and running two DIVA analyses, one ranging from 0° to 360° (on the "original grid"), the other ranging from -180° to 180° (on a "shifted grid"). The two resulting analyses were combined in one on an output grid that extended from 0° to 360° by calculating a weighted average for each grid point, where the weights were proportional to the zonal distance from the central longitude of the respective input grid.

2. In the second iteration, new (artificial) diatom and radiolaria data for SH winter (JAS) were generated at the grid points where diatom and radiolaria data for SH summer (JFM) exist, either using the anomaly with respect to the present observed SST or the gridded data from iteration 1, depending on whether a grid point was assumed to be ice-covered or ice-free for the LGM. We again created seasonal (monthly) data from the February (JFM) and August (JAS) data using a sine function and concatenated all the seasonal (monthly) data as before, but now including the diatom and radiolaria data, and we carried out two more DIVA analyses, one for the original and one for the shifted grid. Finally, the two grids were merged once more following the method of Tyberghein et al. (2012).

3 Results

3.1 Patterns

The monthly maps based on the gridded MARGO SST anomaly clearly exhibit the same basic patterns of SST change as the original MARGO Project Members (2009) synthesis (Fig. 2 and Figs. A1 to A8): Generally, the cooling was larger in the Atlantic than in the Pacific and Indian Oceans. There were strong longitudinal and latitudinal differences in all oceans. The cooling was generally larger in the eastern parts of the oceans than in the western parts and was particularly expressed along the coast of Africa, possibly due to an increase in upwelling or an eastward shift of the coastline and the coastal upwelling systems off Northwest and Southwest Africa (cf. Giraud and Paul, 2010). There was even an 1 °C to 3 °C cooling in the western Pacific warm pool, but overall the east-west temperature differences were less pronounced in the tropical Pacific and Indian Oceans

https://doi.org/10.5194/cp-2019-154
Preprint. Discussion started: 19 February 2020


Climate of the Past Discussions

than in the tropical Atlantic Ocean. A 2 °C to 6 °C cooling in the Southern Ocean may indicate a northward migration of the Polar Front. The apparent warming by 1-2°C of the subtropical gyres in the Pacific Ocean was associated with a rather large uncertainty.

3.2 Global and regional mean changes

Annual averages of the gridded monthly values and their uncertainties were calculated as arithmetic means without any weighting. Global and regional averages (Table 1) and zonal averages (Fig. 3) were calculated from the annually-averaged values as weighted means

$$\overline{T} = \frac{\sum_i w_i T_i}{\sum_i w_i}\,, \tag{1}$$

where the weights were given by

$$w_i = \frac{A_i}{u_i^2} \tag{2}$$

with A_i the area of the ith grid cell and u_i the uncertainty of the gridded value in the ith grid cell. The uncertainties of the global and regional averages were estimated as

$$\overline{u} = \sqrt{\sum_i \left(\frac{w_i}{\sum_i w_i} u_i \right)^2} \times f_{\mathrm{inf}}\,. \tag{3}$$

Here the first factor is the simple sum of the local values of the uncertainty of the gridded field that neglects any spatial covariances (i.e., the non-diagonal terms of the covariance matrix), and the second factor is applied to take into account the missing spatial covariances in an approximate way. According to Troupin et al. (2019), the inflation factor

$$f_{\mathrm{inf}} = \sqrt{\frac{4\pi L^2}{\Delta x \Delta y}} \tag{4}$$

is probably too high, yielding overestimates of the uncertainties. With $L = 10^\circ$ the correlation length of the analysis and $\Delta x = \Delta y = 1^\circ$ the resolution of the grid, in our case the numerical value of the inflation factor was $f_{\mathrm{inf}} = 35.45$.

According to Table 1, the global LGM decrease in the gridded SST was (1.7±0.1) °C. The global tropics (taken to be between 30° S and 30° N) cooled on average by (1.2±0.3) °C, but the tropical Atlantic Ocean by about (1.8±0.6) °C. The cooling in the mid- to high-latitudes was around (3.1±0.2) °C in the North Atlantic Ocean and around (1.4±0.3) °C in the South Alantic Ocean.

3.3 Changes in the meridional differences

The change in the tropical meridional SST difference was calculated as the average SST anomaly between the equator and 30 °N minus the average SST anomaly between 30 °S and the equator (cf. McGee et al., 2014). According to Table 1 and standard uncertainty propagation, this difference decreased by (0.4±0.6) °C for the global ocean and by (0.4±1.2) °C for the Atlantic Ocean.

https://doi.org/10.5194/cp-2019-154
Preprint. Discussion started: 19 February 2020


Climate of the Past Discussions

In contrast, the meridional SST difference between the mid- to high-latitudes in the North Atlantic Ocean (north of 45° N) and the South Atlantic Ocean (south of 30° S - these two regions were chosen in accordance with Rahmstorf, 1996) increased by (1.7±0.3) °C.

3.4 Zonal-mean changes

The zonal mean changes for the global ocean and the Atlantic, Pacific and Indian oceans are shown in Fig. 3. Changes in the Atlantic Ocean were larger than in the other oceans, and changes in the mid- to high latitudes were larger than in the low latitudes, except for the tropical South Atlantic Ocean, where they reached -4 °C due to the cooling in the coastal and equatorial upwelling regions.

3.5 Data-analysis misfit

The normalized data-analysis misfit was determined as

$$J_{\mathrm{misfit}} = \frac{1}{N_{\mathrm{data}}} \sum_i \frac{\left(T_i^{\mathrm{gridded}} - T_i^{\mathrm{data}}\right)^2}{u_i^2} \,, \tag{5}$$

where N_{data} is the number of data-analysis pairs. The normalized misfit was $J_{\mathrm{misfit}} = 1.5$ with $N_{\mathrm{data}} = 420$ for JAS and $J_{\mathrm{misfit}} = 1.7$ with $N_{\mathrm{data}} = 528$ for JFM, respectively. The geographic distribution of the individual misfits at the data locations is shown in Fig. 4. Values larger than the uncertainty of the original data occur in the coastal and equatorial upwelling regions and near and under the reconstructed sea-ice cover.

4 Discussion

The main purpose of our study was to demonstrate the applicability of the DIVA method to sparse paleo data and provide a gridded SST reconstuction for the testing of coupled climate models and forcing of AGCMs. In addition, our gridded data set of LGM SST anomalies allowed us to evaluate changes in global and regional averages and spatial differences including their uncertainties.

Following Eq. 3, we calculated the uncertainties of the global and regional averages as the product of the simple sum of the diagonal terms of the error covariance matrix and an inflation factor, which probably resulted in overestimates. In fact, DIVA may be used to more accurately estimate the spatial covariances as described by the non-diagonal terms, albeit at a much higher computational cost (Troupin et al., 2012; Troupin et al., 2019, Section 4.5; see also Wunsch, 2018). Therefore we decided to use the simplified inflation approach.

As compared to MARGO Project Members (2009, Table 1), our analysis yields SST anomalies for the global ocean and the Atlantic Ocean that tend to be smaller by 0.2 °C to 0.5 °C. The mean change for the global ocean is (-1.7±0.1) °C. The mean change for the tropical Atlantic Ocean of (-2.1±0.7) °C (here for consistency with Schneider von Deimling et al., 2006, taken between 20° S and 20° N) would correspond to an equilibrium climate sensitivity of (1.5±1.0) °C. This is at the low end of the

https://doi.org/10.5194/cp-2019-154
Preprint. Discussion started: 19 February 2020


Climate of the Past Discussions

range from 1.5 °C to 4.5 °C considered to be likely by Collins et al. (2013, Box 12.2), and it is even lower than the estimate by the MARGO Project Members (2009) of (2.3±1.3) °C using the same relationship by Schneider von Deimling et al. (2006, Fig. 6), but based on block-averaged SST anomalies with incomplete coverage.

Our result of a change in the tropical meridional SST difference by (0.41±0.6) °C reflects a greater cooling in the southern tropics than in the northern tropics, mainly due to changes in the coastal and equatorial upwelling regions. It is consistent with the original MARGO synthesis (cf. MARGO Project Members, 2009, Figs. 3 and 4), but inconsistent with, e.g., McGee et al. (2014) who estimate a change of (-0.14±0.18) °C that indicates a greater cooling in the northern tropics than in the southern tropics. According to McGee et al. (2014, Fig. 3), our result would correspond to a northward shift of the ITCZ by (0.8±1.3)° and a decrease of the cross-equatorial heat transport by (0.31±0.5) PW, while McGee et al. (2014) obtain a southward shift by (-0.29±0.38)° and an increase by (0.11±0.14) PW. Part of the differences may be due to our denser data coverage and that we based our calculation of regional averages on a gridded analysis as opposed to single ocean sediment cores or block averages with incomplete coverage. However, we stress that strictly speaking neither our results nor the results by McGee et al. (2014) are statistically significant, because the inferred changes are smaller than their estimated uncertainties.

In contrast, the increase of the meridional SST difference between the mid- to high-latitudes in the North Atlantic Ocean and the South Atlantic Ocean of (1.7±0.3) °C is statistically significant and by itself would argue for an intensified Atlantic meridional overturning circulation, which is indeed found in some simulations of the LGM ocean circulation (e.g., Kurahashi-Nakamura et al., 2017). However, this increase may be counteracted by an accompanying decrease of the sea-surface salinity gradient, which may result in an overall decrease of the sea-surface density gradient (e.g., Paul and Schäfer-Neth, 2003). Both the decrease of the tropical meridional SST difference and the increase of the large-scale Atlantic meridional SST difference are also evident from the zonal-mean SST changes in Fig. 3.

The normalized misfits of $J_{\mathrm{misfit}} = 1.5$ for JAS and $J_{\mathrm{misfit}} = 1.7$ for JFM mean that on average the misfit was larger than the uncertainty of the original data by 50 % to 70 %. However, the geographic distribution shows that large misfits were restricted to certain regions (e.g., subject to large variations due to upwelling or sea-ice cover) and maybe due to deviations between near-by sediment core locations.

We deliberately made use of the separate summer and winter temperature reconstructions based on the faunal transfer function technique. This technique may not provide fully independent seasonally resolved SST reconstructions (cf. Mix et al., 2001; Morey et al., 2005) but partly reflect the seasonal SST structure of the calibration data set (Kucera et al., 2005b), as indicated by the very high correlation (r≈0.94) between the seasonal reconstructions and the winter and summer SST in the calibration data sets (Kucera et al., 2005b). However, we are confident that some information on the amplitude of the seasonal cycle may still be inferred from microfossil abundances using the faunal transfer function technique as long as both warmth- and cold-loving species are present and no-analog situations are avoided.

https://doi.org/10.5194/cp-2019-154
Preprint. Discussion started: 19 February 2020


Climate of the Past Discussions
Open Access
EGU

5 Conclusions

We found that the Data-Interpolating Variational Analysis (DIVA Troupin et al., 2012) method, which has so far been applied to comparatively dense oceanographic observations, was also capable of analyzing much sparser paleoceanographic reconstructions at irregularly spaced ocean sediment core locations. Using DIVA, we derived a climatology of the monthly SST and sea-ice extent during the LGM on a global $1° \times 1°$ grid as an extension of the GLAMAP reconstruction of Atlantic SST (Sarnthein et al., 2003), based on MARGO microfossil assemblages (Kucera et al., 2005a) and a number of sea-ice reconstructions. This gridded climatology confirmed that the longitudinal and meridional SST differences were greater than today, as previously proposed by the MARGO project. Furthermore, we were able to calculate global and regional averages, using the uncertainty estimate provided by DIVA as a weight, and we quantified the meridional SST differences. In addition, we estimated the uncertainties of the global and regional averages and the meridional SST differences. For the equilibrium climate sensitivity of the LGM, we obtained an estimate of (1.5±1.0) °C at the low end of the range considered to be likely by Collins et al. (2013).

6 Outlook

We expect the Glacial Ocean Map (GLOMAP) to prove useful in evaluating coupled climate models and forcing AGCMs in simulations of the climate of the LGM. Furthermore, it may be compared to data assimilation (e.g., Annan and Hargreaves, 2013) or state estimation efforts (e.g., Kurahashi-Nakamura et al., 2017), which yield a seasonal SST field that is consistent with the underlying "(model) physics" of the ocean circulation and climate, but at a computational cost that is larger by two or more orders of magnitude. In turn, the gridded field and error estimate provided by DIVA may allow to first smooth and spread the original sparse data before using it in constraining an inverse model (cf. Marchal and Curry, 2008).

Finally, we plan to use water isotopes as a tool to compare the performance of different AGCMs, using our gridded GLOMAP SST climatology as a boundary condition. This way we can on the one hand avoid the propagation of the SST bias in coupled climate models, and on the other hand we can isolate the impact of the ocean feedback on the simulated distributions of water isotopes over land, ice and ocean (e.g., Werner et al., 2018). We also plan to extend our method to δ^{18}O from fossil calcite shells of planktonic foraminifera. A combined reconstruction of SST, sea ice coverage and the inferred δ^{18}O of sea water may be used for an enhanced evaluation of coupled climate models.

Data availability. The GLOMAP gridded climatology of monthly LGM SST anomalies (including their uncertainties) and monthly estimates of LGM sea-ice extent will be made available through PANGAEA (https://www.pangaea.de). It may be updated when new reconstructions become available.

Competing interests. The authors declare that they have no conflict of interest.

https://doi.org/10.5194/cp-2019-154
Preprint. Discussion started: 19 February 2020

Acknowledgements. This work was supported by the German Federal Ministry of Education and Research (BMBF) as a Research for Sustainability initiative (FONA) through the PalMod project (FKZ: 01LP1511D) as well as by the DFG Research Center/Center of Excellence MARUM – "The Ocean in the Earth System".

https://doi.org/10.5194/cp-2019-154
Preprint. Discussion started: 19 February 2020

Climate of the Past Discussions

References

Annan, J. D. and Hargreaves, J. C.: A new global reconstruction of temperature changes at the Last Glacial Maximum, Climate of the Past, 9, 367–376, https://doi.org/10.5194/cp-9-367-2013, 2013.

Briggs, R. D., Pollard, D., and Tarasov, L.: A data-constrained large ensemble analysis of Antarctic evolution since the Eemian, Quaternary Science Reviews, 103, 91–115, https://doi.org/10.1016/j.quascirev.2014.09.003, 2014.

CLIMAP Project Members: Seasonal reconstructions of the Earth's surface at the Last Glacial Maximum, Geological Society of America, Map and Chart Series, MC-36, 1–18, 1981.

Collins, M., Knutti, R., Arblaster, J., Dufresne, J.-L., Fichefet, T., Friedlingstein, P., Gao, X., Gutowski, W., Johns, T., Krinner, G., Shongwe, M., Tebaldi, C., Weaver, A., and Wehner, M.: Long-term Climate Change: Projections, Commitments and Irreversibility, in: Climate Change 2013: The Physical Science Basis. Contribution of Working Group I to the Fifth Assessment Report of the Intergovernmental Panel on Climate Change, edited by Stocker, T., Qin, D., Plattner, G.-K., Tignor, M., Allen, S., Boschung, J., Nauels, A., Xia, Y., Bex, V., and Midgley, P., pp. 1029–1136, Cambridge University Press, 2013.

de Vernal, A., Eynaud, F., Henry, M., Hillaire-Marcel, C., Londeix, L., Mangin, S., Mathiessen, J., Marret, F., Radi, T., Rochon, A., Solignac, S., and Turon, J.-L.: Reconstruction of sea-surface conditions at middle to high latitudes of the Northern Hemisphere during the Last Glacial Maximum (LGM) based on dinoflagellate cyst assemblages, Quaternary Science Reviews, 24, 897–924, https://doi.org/10.1016/j.quascirev.2004.06.014, 2005.

De Vernal, A., Rosell-Melé, A., Kucera, M., Hillaire-Marcel, C., Eynaud, F., Weinelt, M., Dokken, T., and Kageyama, M.: Comparing proxies for the reconstruction of LGM sea-surface conditions in the northern North Atlantic, Quaternary Science Reviews, 25, 2820–2834, https://doi.org/10.1016/j.quascirev.2006.06.006, 2006.

Eisenman, I.: Geographic muting of changes in the Arctic sea ice cover, Geophysical Research Letters, 37, https://doi.org/10.1029/2010GL043741, 2010.

Gersonde, R., Crosta, X., Abelmann, A., and Armand, L.: Sea-surface temperature and sea ice distribution of the Southern Ocean at the EPILOG Last Glacial Maximum—a circum-Antarctic view based on siliceous microfossil records, Quaternary Science Reviews, 24, 869–896, https://doi.org/doi:10.1016/j.quascirev.2004.07.015, 2005.

Giraud, X. and Paul, A.: Interpretation of the paleo–primary production record in the NW African coastal upwelling system as potentially biased by sea level change, Paleoceanography, 25, https://doi.org/10.1029/2009PA001795, 2010.

Jansen, E., Overpeck, J., Briffa, K., Duplessy, J.-C., Joos, F., Masson-Delmotte, V., Olago, D., Otto-Bliesner, B., Peltier, W., Rahmstorf, S., Ramesh, R., Raynaud, D., Rind, D., Solomina, O., Villalba, R., and Zhang, D.: Palaeoclimate, in: Climate Change 2007: The Physical Science Basis. Contribution of Working Group I to the Fourth Assessment Report of the Intergovernmental Panel on Climate Change, edited by Solomon, S., Qin, D., Manning, M., Chen, Z., Marquis, M., Averyt, K., Tignor, M., and Miller, H., pp. 447–451, Cambridge University Press, Cambridge, United Kingdom and New York, NY, USA, 2007.

Kageyama, M., Albani, S., Braconnot, P., Harrison, S. P., Hopcroft, P. O., Ivanovic, R. F., Lambert, F., Marti, O., Peltier, W. R., Peterschmitt, J.-Y., Roche, D. M., Tarasov, L., Zhang, X., Brady, E. C., Haywood, A. M., LeGrande, A. N., Lunt, D. J., Mahowald, N. M., Mikolajewicz, U., Nisancioglu, K. H., Otto-Bliesner, B. L., Renssen, H., Tomas, R. A., Zhang, Q., Abe-Ouchi, A., Bartlein, P. J., Cao, J., Li, Q., Lohmann, G., Ohgaito, R., Shi, X., Volodin, E., Yoshida, K., Zhang, X., and Zheng, W.: The PMIP4 contribution to CMIP6 – Part 4: Scientific objectives and experimental design of the PMIP4-CMIP6 Last Glacial Maximum experiments and PMIP4 sensitivity experiments, Geoscientific Model Development, 10, 4035–4055, https://doi.org/10.5194/gmd-10-4035-2017, 2017.

https://doi.org/10.5194/cp-2019-154
Preprint. Discussion started: 19 February 2020

Kucera, M., Rosell-Melé, A., Schneider, R., Waelbroeck, C., and Weinelt, M.: Multiproxy approach for the reconstruction of the glacial ocean surface (MARGO), Quaternary Science Reviews, 24, 813–819, 2005a.

Kucera, M., Weinelt, M., Kiefer, T., Pflaumann, U., Hayes, A., Weinelt, M., Chen, M.-T., Mix, A. C., Barrows, T. T., Cortijo, E., Duprat, J., Juggins, S., and Waelbroeck, C.: Reconstruction of sea-surface temperatures from assemblages of planktonic foraminifera: Multi-technique approach based on geographically constrained calibration data sets and its application to glacial Atlantic and Pacific Oceans, Quaternary Science Reviews, 24, 951–998, https://doi.org/doi:10.1016/j.quascirev.2004.07.014, 2005b.

Kurahashi-Nakamura, T., Paul, A., and Losch, M.: Dynamical reconstruction of the global ocean state during the Last Glacial Maximum, Paleoceanography, 32, 326–350, https://doi.org/10.1002/2016PA003001, 2017.

Marchal, O. and Curry, W. B.: On the Abyssal Circulation in the Glacial Atlantic, Journal of Physical Oceanography, 38, 2014–2037, https://doi.org/doi: 10.1175/2008JPO3895.1, 2008.

MARGO Project Members: Constraints on the magnitude and patterns of ocean cooling at the Last Glacial Maximum, Nature Geoscience, 2, 127–132, doi:10.1039/NGEO411, 2009.

Masson-Delmotte, V., Schulz, M., Abe-Ouchi, A., Beer, J., Ganopolski, A., González Rouco, J., Jansen, E., Lambeck, K., Luterbacher, J., Naish, T., Osborn, T., Otto-Bliesner, B., Quinn, T., Ramesh, R., Rojas, M., Shao, X., and Timmermann, A.: Information from Paleoclimate Archives, in: Climate Change 2013: The Physical Science Basis. Contribution of Working Group I to the Fifth Assessment Report of the Intergovernmental Panel on Climate Change, edited by Stocker, T., Qin, D., Plattner, G.-K., Tignor, M., Allen, S., Boschung, J., Nauels, A., Xia, Y., Bex, V., and Midgley, P., pp. 383–464, Cambridge University Press, Cambridge, United Kingdom and New York, NY, USA, 2013.

McGee, D., Donohoe, A., Marshall, J., and Ferreira, D.: Changes in ITCZ location and cross-equatorial heat transport at the Last Glacial Maximum, Heinrich Stadial 1, and the mid-Holocene, Earth and Planetary Science Letters, 390, 69–79, https://doi.org/10.1016/j.epsl.2013.12.043, 2014.

Méheust, M., Ruediger Stein, R., Fahl, K., Max, L., and Riethdorf, J. R.: High-resolution IP25-based reconstruction of sea-ice variability in the western North Pacific and Bering Sea during the past 18,000 years, Geo-Marine Letters, 36, 101–111, https://doi.org/10.1007/s00367-015-0432-4, 2016.

Méheust, M., Ruediger Stein, R., Fahl, K., and Gersonde, R.: Sea-ice variability in the subarctic North Pacific and adjacent Bering Sea during the past 25 ka: new insights from IP25 and $U^{k'}_{37}$ proxy records, Arktos, 4, https://doi.org/10.1007/s41063-018-0043-1, 2018.

Mix, A. C., Bard, E., and Schneider, R.: Environmental processes of the ice age: Land, oceans, glaciers (EPILOG), Quaternary Science Reviews, 20, 627–658, 2001.

Morey, A. E., Mix, A. C., and Pisias, N. G.: Planktonic foraminiferal assemblages preserved in surface sediments correspond to multiple environmental variables, Quaternary Science Reviews, 24, 951–998, https://doi.org/10.1016/j.quascirev.2003.09.011, 2005.

Paul, A. and Schäfer-Neth, C.: Modeling the water masses of the Atlantic Ocean at the Last Glacial Maximum, Paleoceanography, 18, doi:10.1029/2002PA000 783, 2003.

Rahmstorf, S.: On the freshwater forcing and transport of the North Atlantic thermohaline circulation, Climate Dynamics, 12, 799–811, 1996.

Roche, D. M., Crosta, X., and Renssen, H.: Evaluating Southern Ocean sea-ice for the Last Glacial Maximum and pre-industrial climates: PMIP-2 models and data evidence, Quaternary Science Reviews, 56, 99–106, https://doi.org/10.1016/j.quascirev.2012.09.020, 2012.

Sarnthein, M., Gersonde, R., Niebler, S., Pflaumann, U., Spielhagen, R., Thiede, J., Wefer, G., and Weinelt, M.: Overview of Glacial Atlantic Ocean Mapping (GLAMAP 2000), Paleoceanography, 18, doi:10.1029/2002PA00 769, 2003.

https://doi.org/10.5194/cp-2019-154
Preprint. Discussion started: 19 February 2020

Schäfer-Neth, C. and Paul, A.: The Atlantic Ocean at the Last Glacial Maximum: 1. Objective mapping of the GLAMAP sea-surface conditions, in: The South Atlantic in the Late Quaternary: Reconstruction of Material Budgets and Current Systems, edited by Wefer, G., Mulitza, S., and Ratmeyer, V., pp. 531–548, Springer-Verlag, Berlin, Heidelberg, 2004.

Schäfer-Neth, C., Paul, A., and Mulitza, S.: Perspectives on mapping the MARGO reconstructions by variogram analysis/kriging and objective analysis, Quaternary Science Reviews, 23, 1083–1093, doi:10.1016/j.quascirev.2004.06.017, 2005.

Schneider von Deimling, T., Held, H., Ganopolski, A., and Rahmstorf, S.: Climate sensitivity estimated from ensemble simulations of glacial climate, Climate Dynamics, 27, 149–163, doi:10.1007/s00 382–006–0126–8, 2006.

Tarasov, L., Dyke, A. S., Neal, R. M., and Peltier, W. R.: A data-calibrated distribution of deglacial chronologies for the North American ice complex from glaciological modeling, EPSL, 315-316, 30–40, https://doi.org/10.1016/j.epsl.2011.09.010, 2012.

Troupin, C., Barth, A., Sirjacobs, D., Ouberdous, M., Brankart, J.-M., Brasseur, P., Rixen, M., Alvera-Azcárate, A., Belounis, M., Capet, A., Lenartz, F., Toussaint, M.-E., and Beckers, J.-M.: Generation of analysis and consistent error fields using the Data Interpolating Variational Analysis (DIVA), Ocean Modelling, 52-53, 90–101, https://doi.org/10.1016/j.ocemod.2012.05.002, http://modb.oce.ulg.ac.be, 2012.

Troupin, C., Watelet, S., Ouberdous, M., Sirjacobs, D., Alvera-Azcárate, A., Barth, A., Toussaint, M.-E., and Beckers, J.-M.: Data Interpolating Variational Analysis User Guide, Tech. rep., GeoHydrodynamics and Environment Research (GHER), Departement of Astrophysics, Geophysics and Oceanography, University of Liège, http://modb.oce.ulg.ac.be, 2019.

Tyberghein, L., Verbruggen, H., Pauly, K., Troupin, C., Mineur, F., and De Clerck, O.: Bio-ORACLE: a global environmental dataset for marine species distribution modelling, Global Ecology and Biogeography, 21, 272–281, https://doi.org/10.1111/j.1466-8238.2011.00656.x, 2012.

Werner, M., Jouzel, J., Masson-Delmotte, V., and Lohmann, G.: Reconciling glacial Antarctic water stable isotopes with ice sheet topography and the isotopic paleothermometer, Nature Communications, 9, 3537, https://doi.org/doi:10.1038/s41467-018-05430-y, 2018.

WOA: World Ocean Atlas 1998, Tech. rep., National Oceanographic Data Center, Silver Spring, Maryland, 1998.

Wunsch, C.: Towards determining uncertainties in global oceanic mean values of heat, salt, and surface elevation, Tellus A: Dynamic Meteorology and Oceanography, 70, 1–14, https://doi.org/10.1080/16000870.2018.1471911, 2018.

Xiao, X., Stein, R., and Fahl, K.: MIS 3 to MIS 1 temporal and LGM spatial variability in Arctic Ocean sea ice cover: Reconstruction from biomarkers, Paleoceanography, 30, 969–983, https://doi.org/10.1002/2015PA002814, 2015.

https://doi.org/10.5194/cp-2019-154
Preprint. Discussion started: 19 February 2020

Climate of the Past Discussions

Table 1. Global and regional averages and meridional differences of SST anomalies (LGM - modern) based on data gridded with DIVA and weighted by their uncertainties.

GLOMAP regional averages, meridional differences and uncertainties		
Region	Average	Uncertainty
Global ocean	-1.7	0.1
Global tropical ocean (30° S - 30° N)	-1.2	0.3
Northern tropical ocean (0° - 30° N)	-0.9	0.4
Southern tropical ocean (30° S - 0°)	-1.4	0.4
Tropical meridional difference (north - south)	0.4	0.6
Tropical Atlantic Ocean (30° S - 30° N)	-1.8	0.6
Tropical Atlantic Ocean (20° S - 20° N)	-2.1	0.7
Northern Tropical Atlantic Ocean	-1.6	0.8
Southern Tropical Atlantic Ocean	-2.0	0.8
Tropical Atlantic meridional difference	0.4	1.2
Northern North Atlantic Ocean (> 45° N)	-3.1	0.2
Southern South Atlantic Ocean (< -30° S)	-1.4	0.3
Atlantic meridional difference (north - south)	-1.7	0.3

All temperature anomalies and uncertainties in units of °C

https://doi.org/10.5194/cp-2019-154
Preprint. Discussion started: 19 February 2020

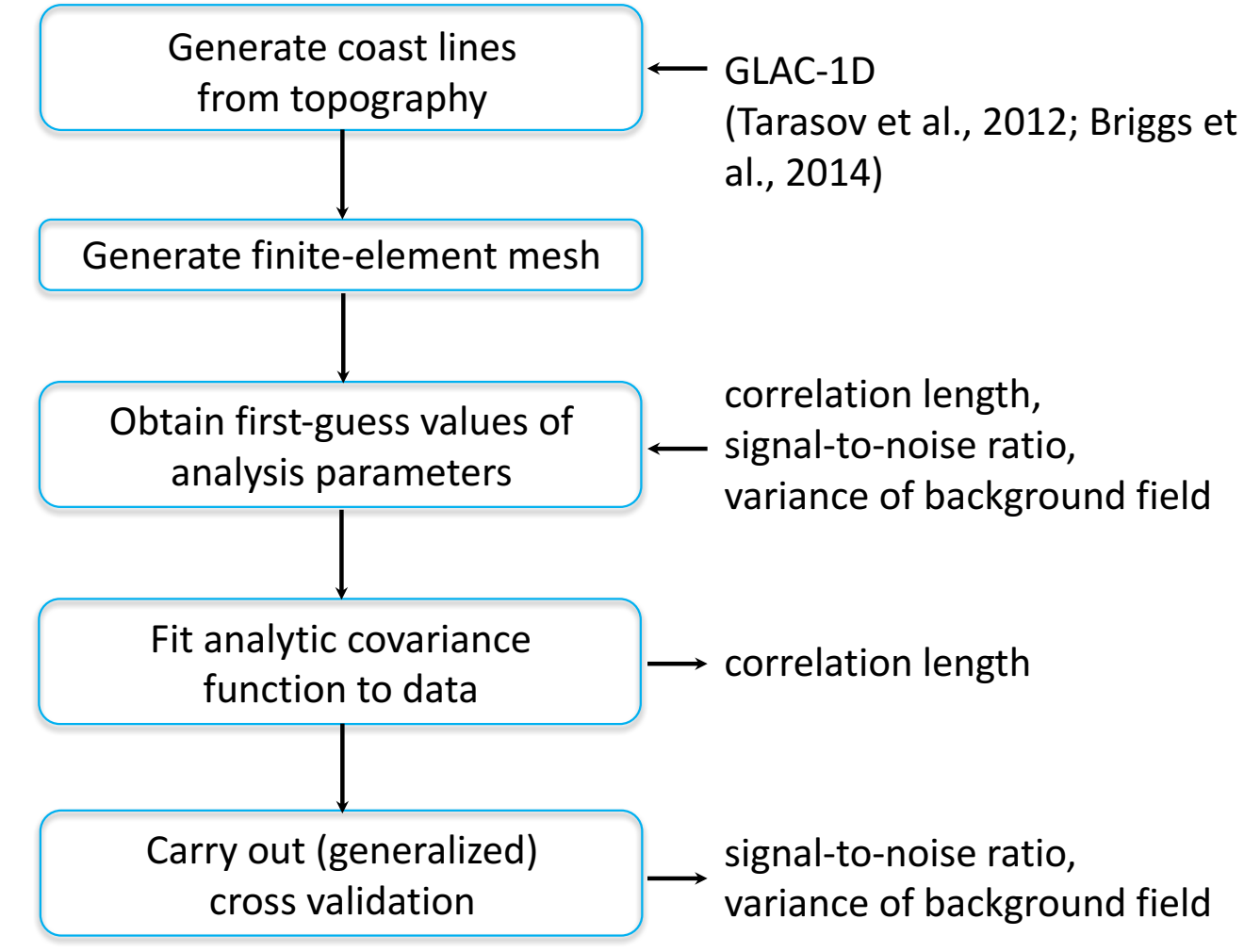

Figure 1. General workflow of DIVA (Data-Interpolating Variational Analysis, Troupin et al.,2012).

https://doi.org/10.5194/cp-2019-154
Preprint. Discussion started: 19 February 2020

Climate of the Past
Discussions
Open Access
EGU

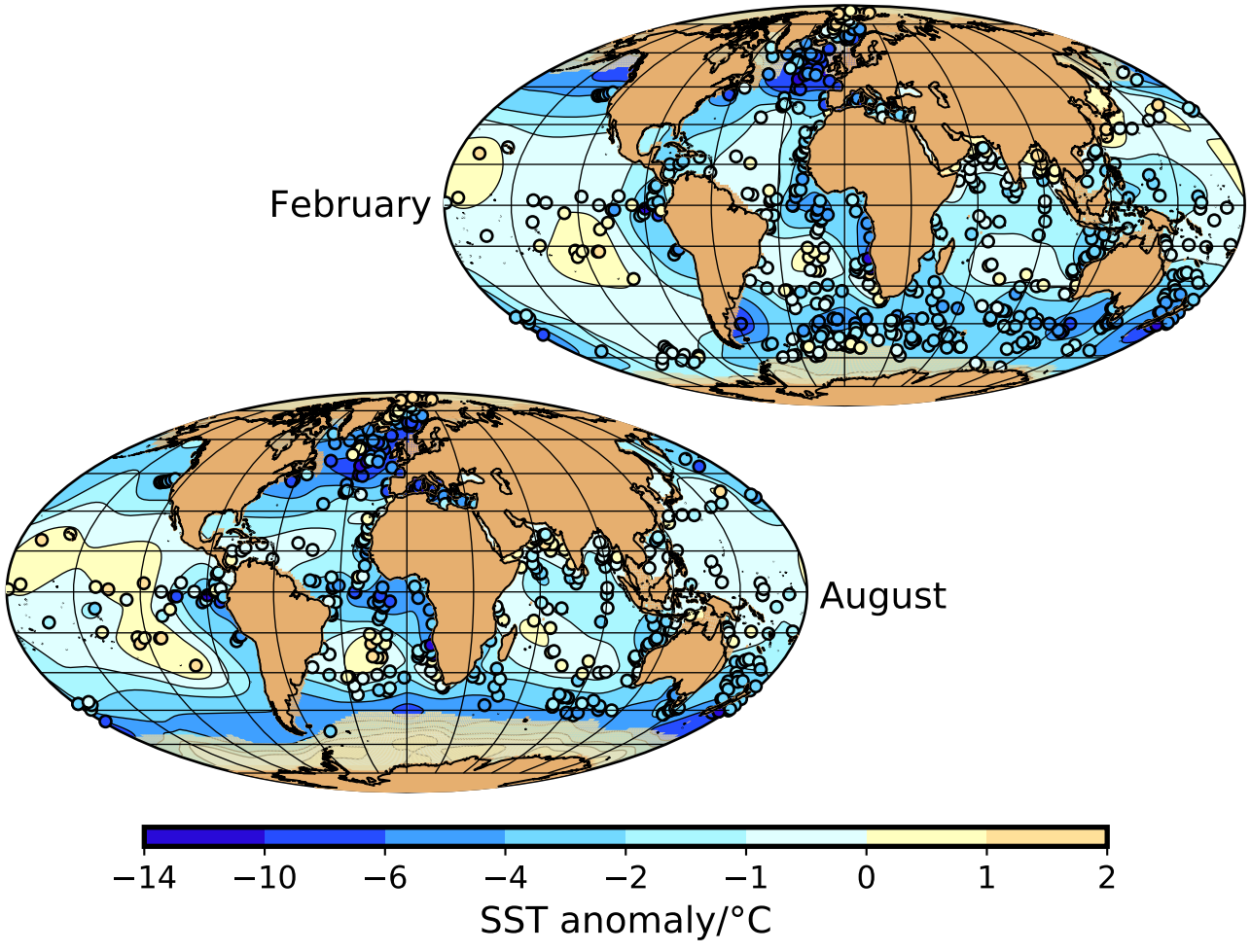

Figure 2. Analyzed SST anomalies for February and August (contour map) and data values (colored circles).

https://doi.org/10.5194/cp-2019-154
Preprint. Discussion started: 19 February 2020

Climate of the Past Discussions
Open Access
EGU

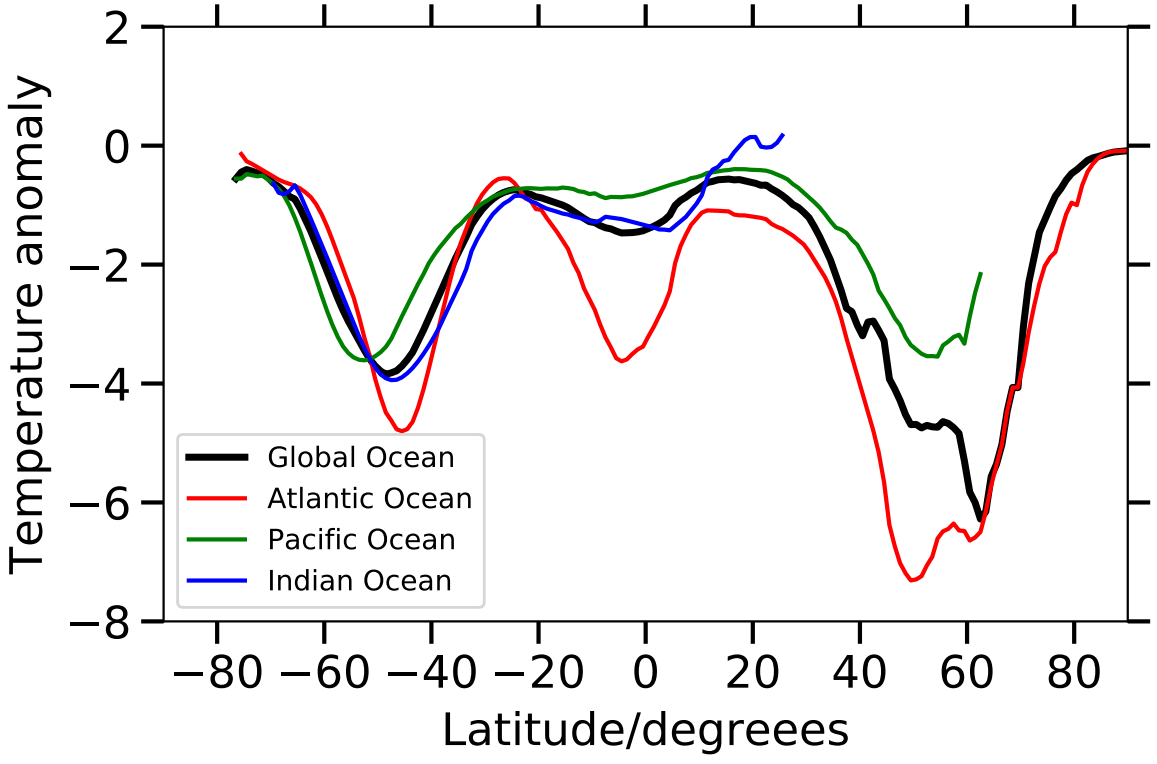

Figure 3. Zonally-averaged annual-mean SST anomalies for the global ocean, Atlantic Ocean, Pacific Ocean and Indian Ocean.

https://doi.org/10.5194/cp-2019-154
Preprint. Discussion started: 19 February 2020

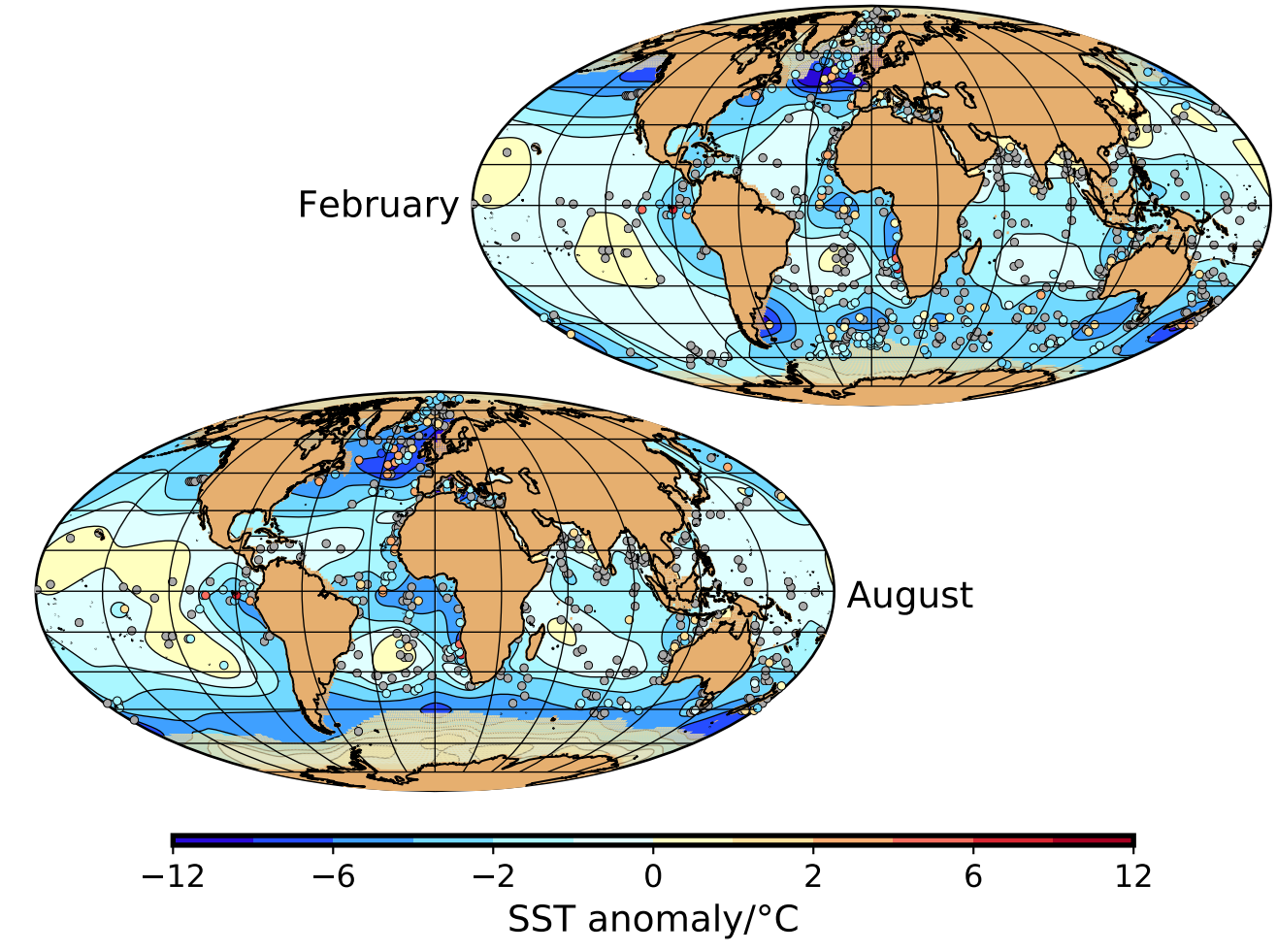

Figure 4. Analyzed SST anomalies for February and August (contour map) and differences between the gridded values and the block-averaged original data values (colored circles – differences smaller than the uncertainty of the data are shown in dark grey.).

https://doi.org/10.5194/cp-2019-154
Preprint. Discussion started: 19 February 2020

Climate of the Past Discussions
Open Access
EGU

Appendix A: Maps of monthly SST anomalies and their estimated uncertainties

https://doi.org/10.5194/cp-2019-154
Preprint. Discussion started: 19 February 2020

Climate of the Past
Discussions
Open Access
EGU

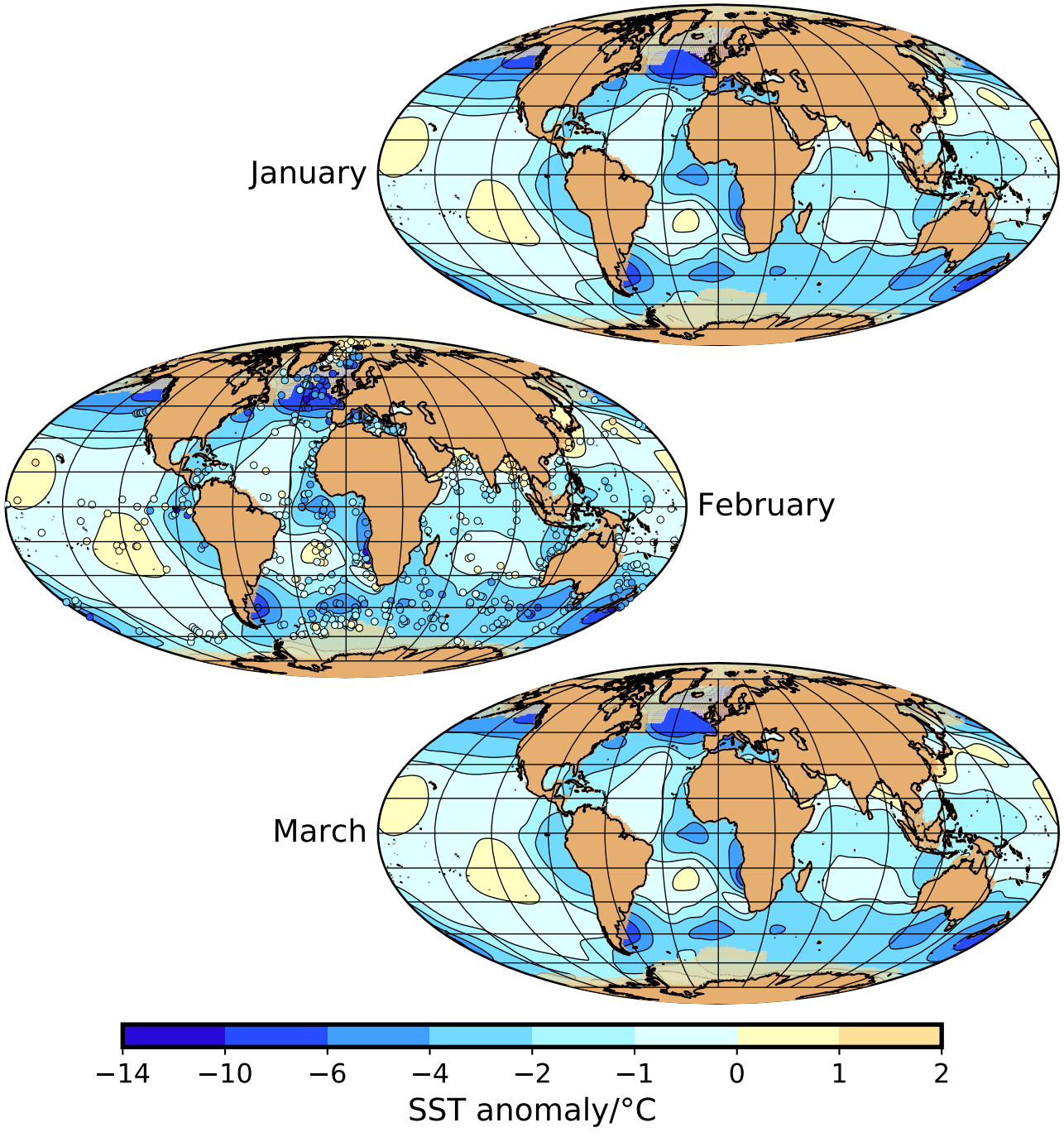

Figure A1. Sea-surface temperature anomaly and sea-ice extent for January, February and March. For February, we also show the MARGO reconstruction at the sediment core locations.

https://doi.org/10.5194/cp-2019-154
Preprint. Discussion started: 19 February 2020

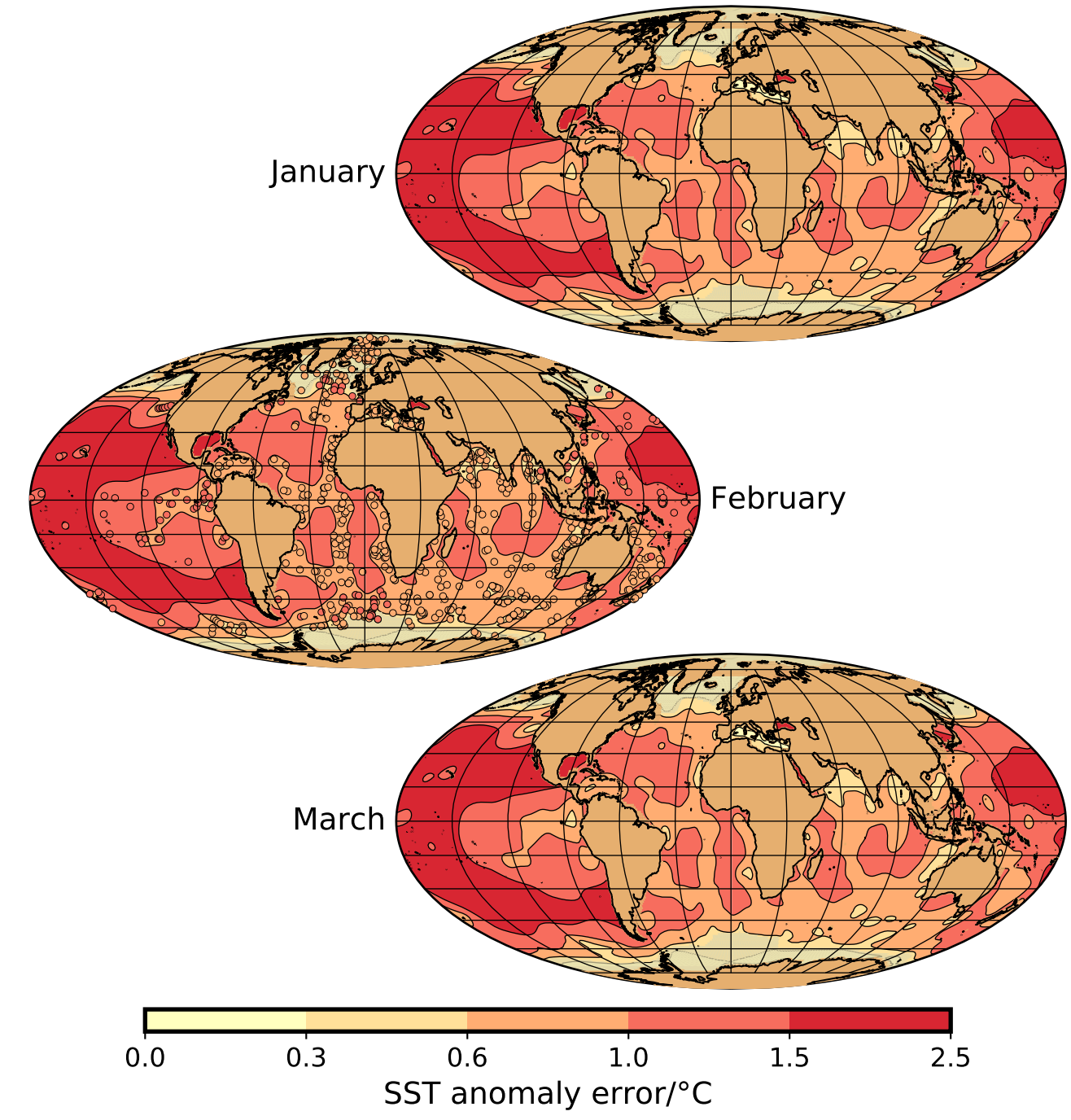

Figure A2. Uncertainty of SST anomaly for January, February and March. For February, we also show the estimated error of the MARGO reconstruction at the sediment core locations.

https://doi.org/10.5194/cp-2019-154
Preprint. Discussion started: 19 February 2020

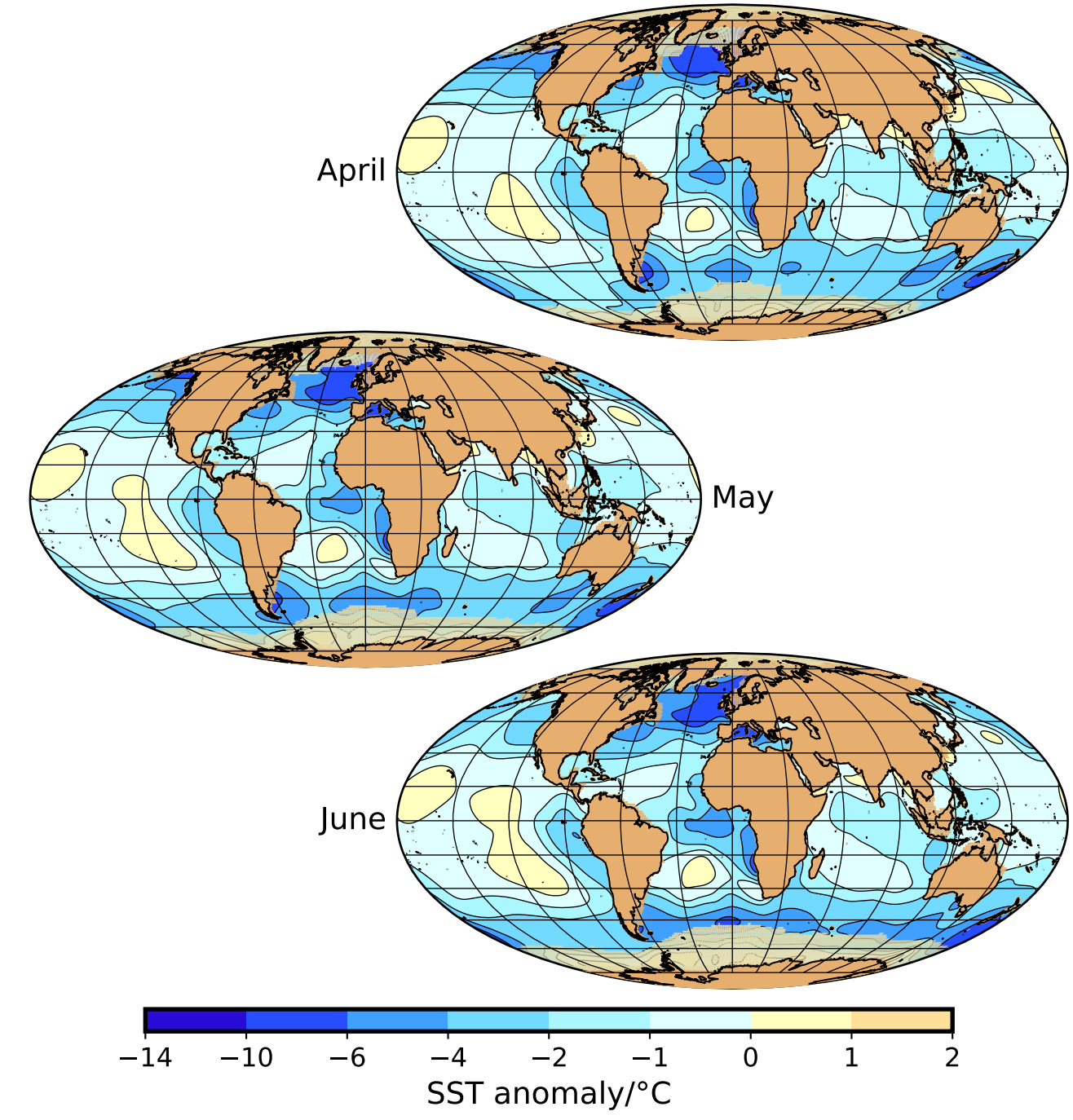

Figure A3. Sea-surface temperature anomaly and sea-ice extent for April, May and June

https://doi.org/10.5194/cp-2019-154
Preprint. Discussion started: 19 February 2020

Climate of the Past
Discussions
Open Access
EGU

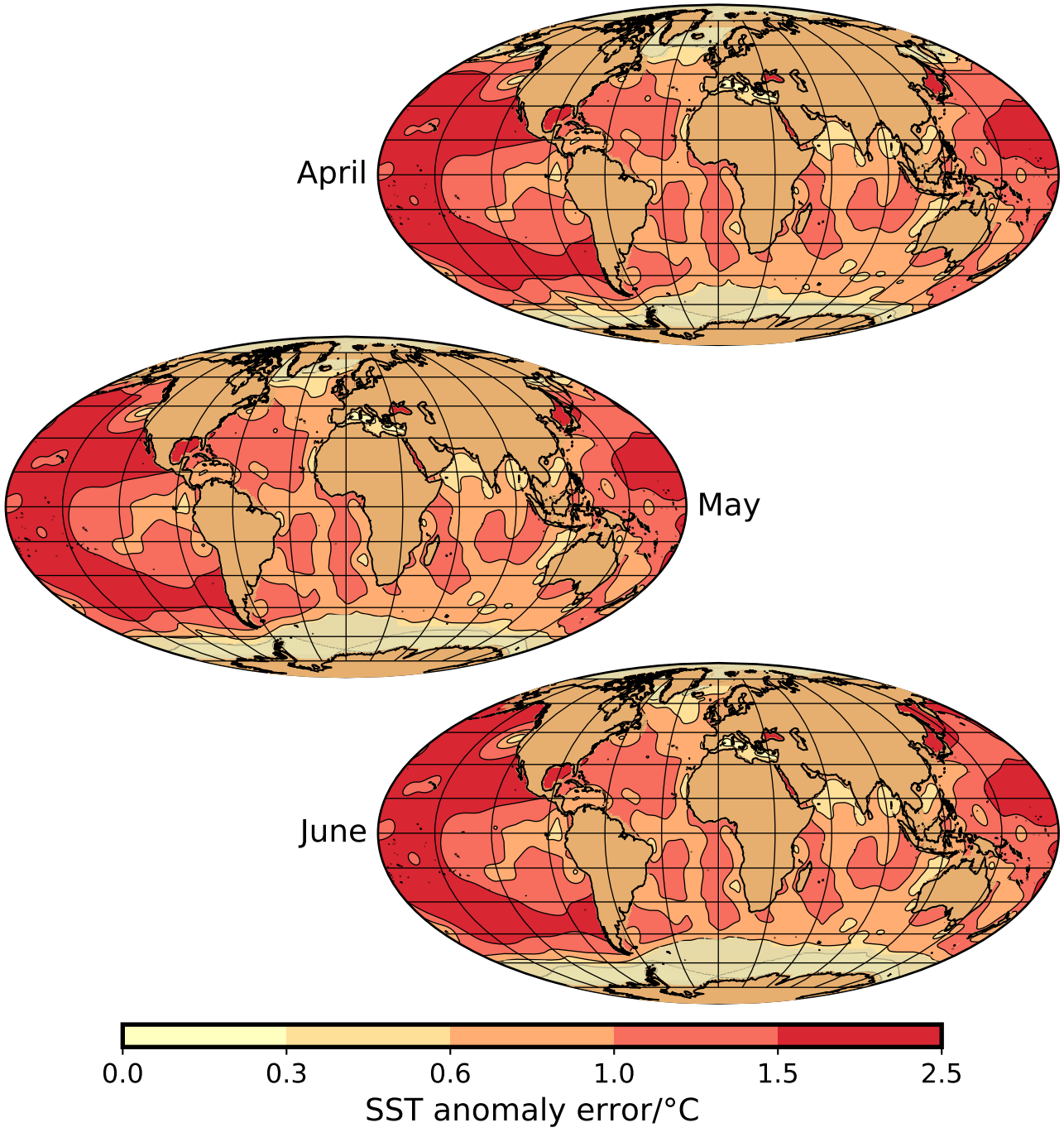

Figure A4. Uncertainty of SST anomaly for April, May and June

https://doi.org/10.5194/cp-2019-154
Preprint. Discussion started: 19 February 2020

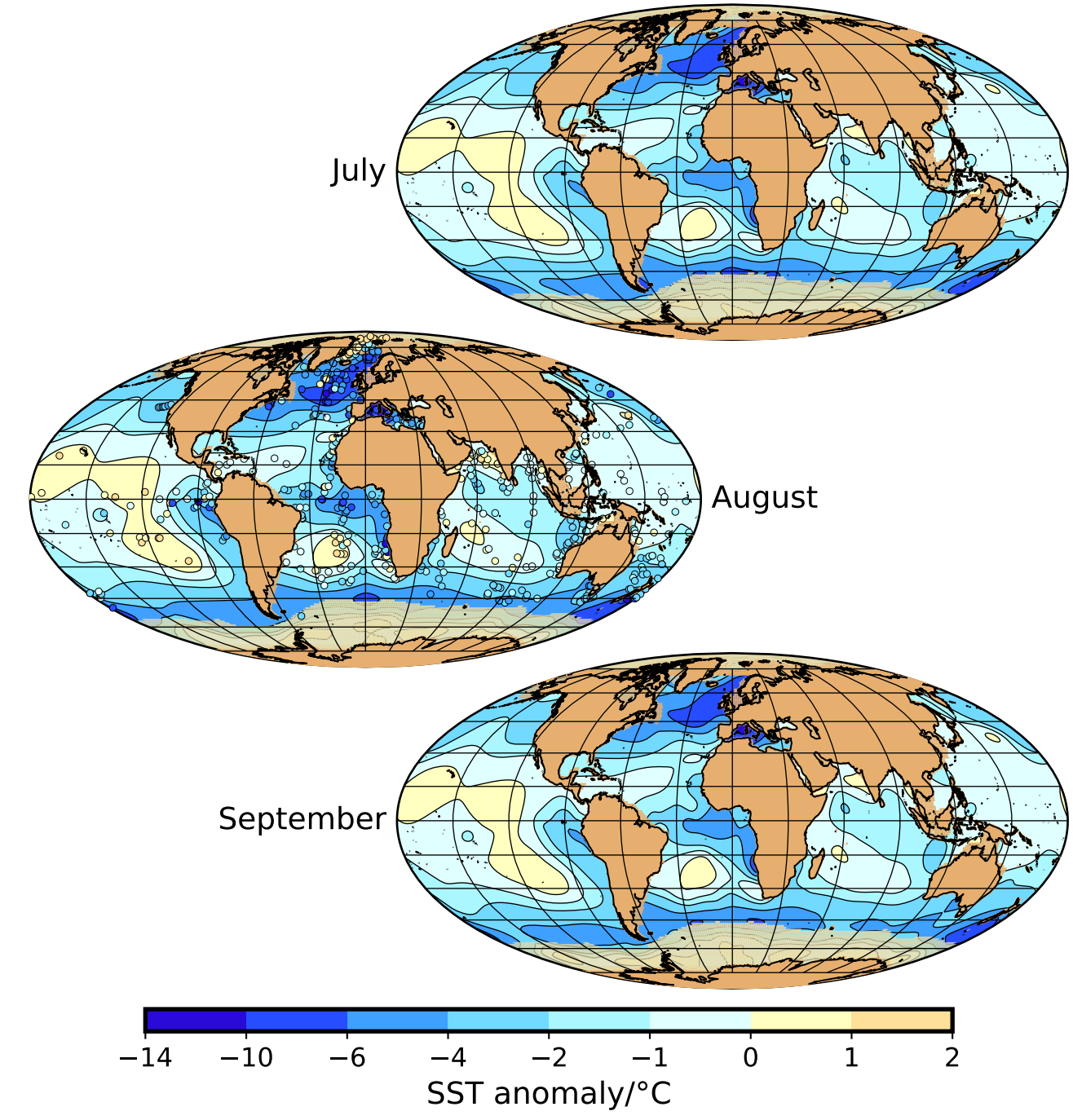

Figure A5. Sea-surface temperature anomaly and sea-ice extent for July, August and September. For August, we also show the MARGO reconstruction at the sediment core locations.

https://doi.org/10.5194/cp-2019-154
Preprint. Discussion started: 19 February 2020

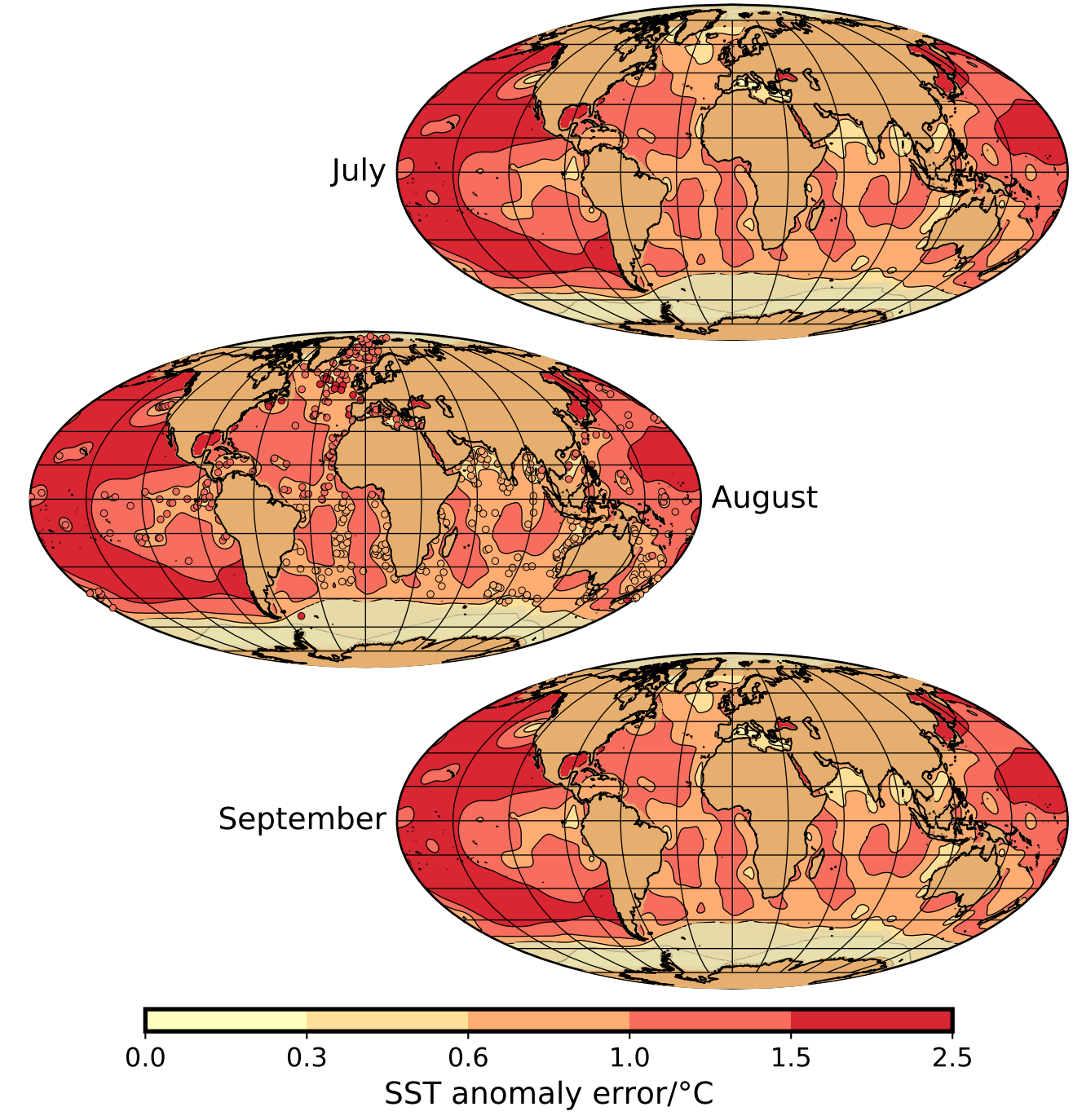

Figure A6. Uncertainty of SST anomaly for July, August and September. For August, we also show the estimated error of the MARGO reconstruction at the sediment core locations.

https://doi.org/10.5194/cp-2019-154
Preprint. Discussion started: 19 February 2020

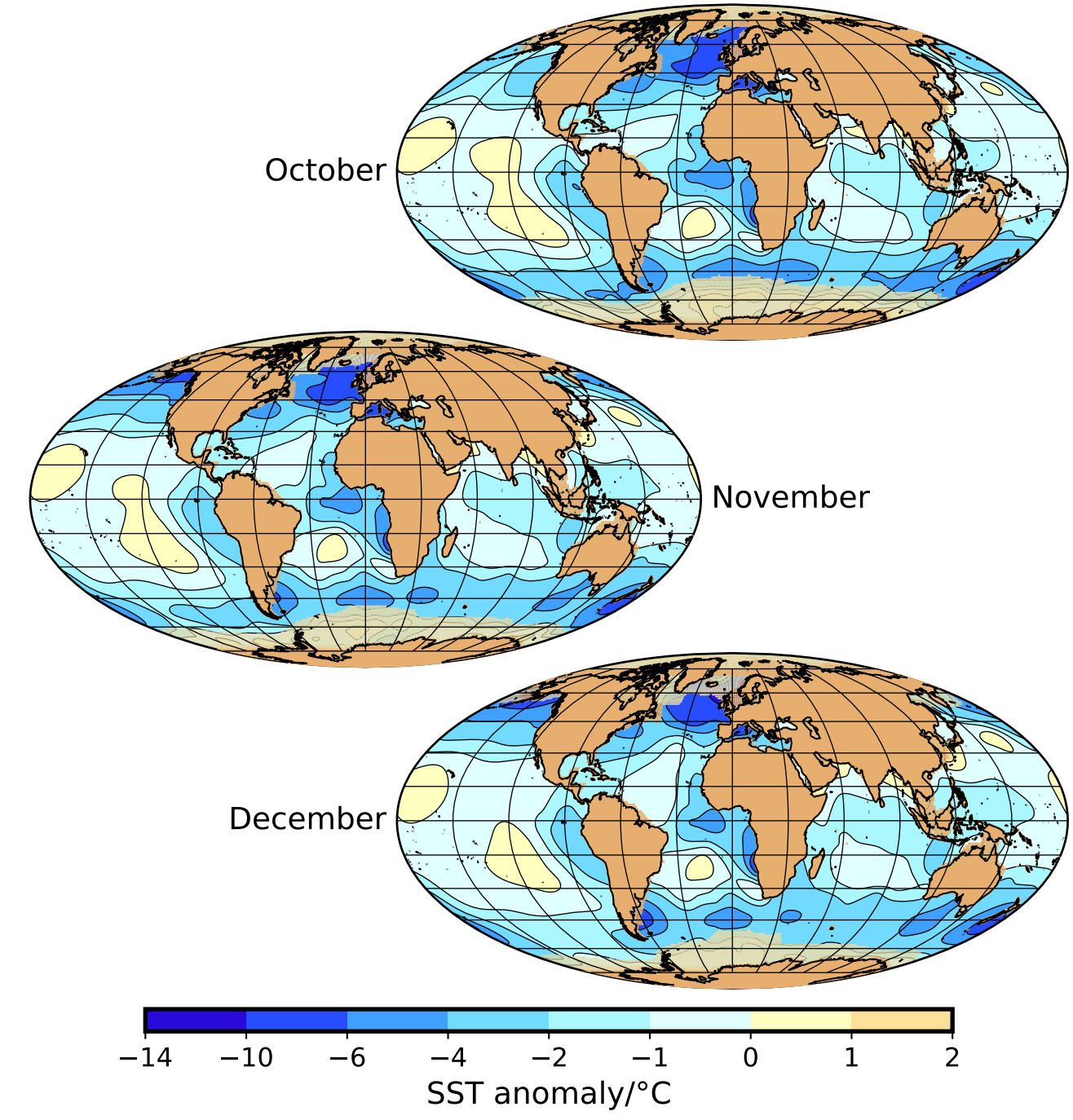

Figure A7. Sea-surface temperature anomaly and sea-ice extent for October, November and December

https://doi.org/10.5194/cp-2019-154
Preprint. Discussion started: 19 February 2020

Climate of the Past
Discussions
Open Access
EGU

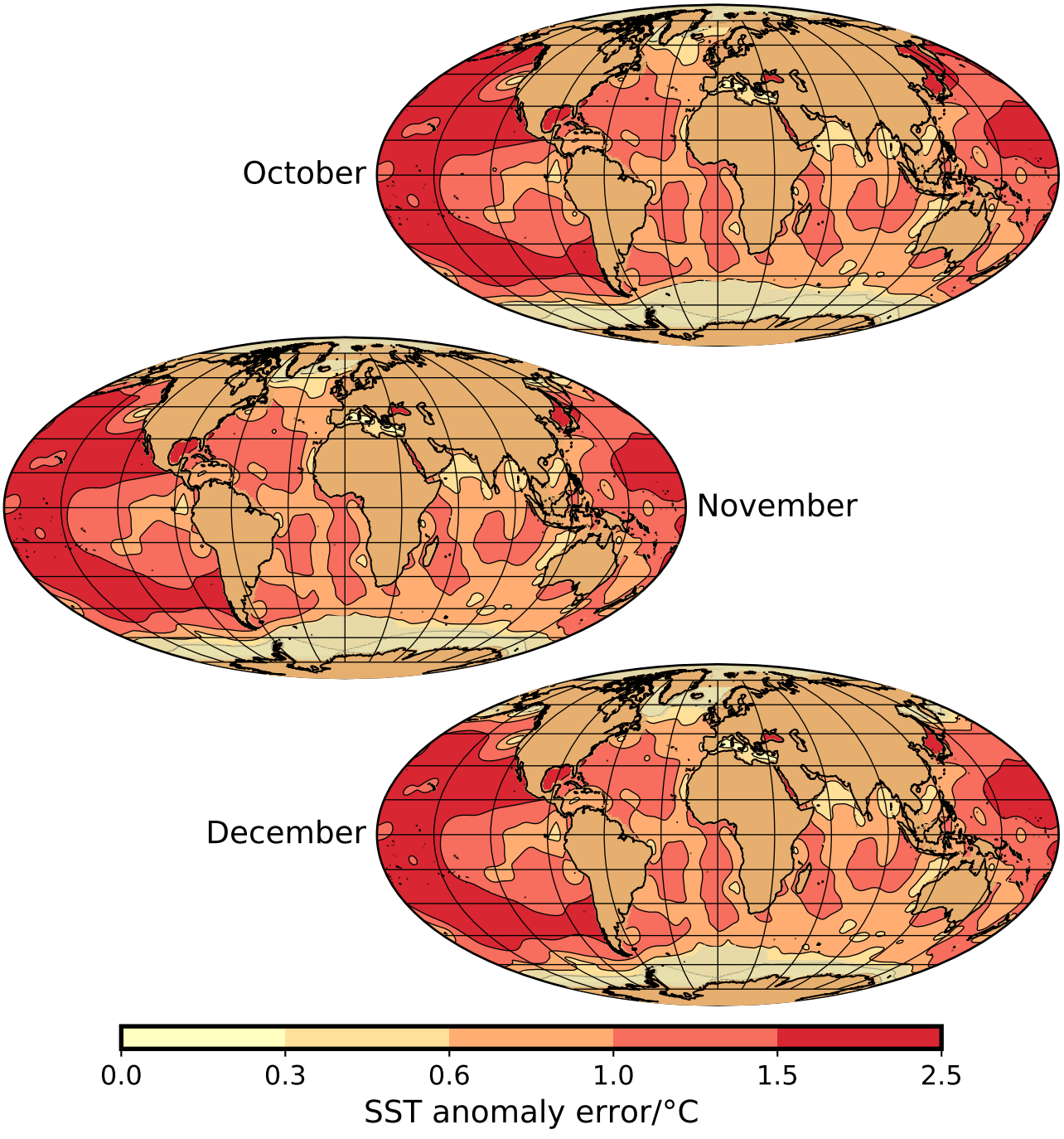

Figure A8. Uncertainty of SST anomaly for October, November and December